1 **Title**

2 Estimating animal density in three dimensions using capture-frequency data from remote detectors

3 **Authors and affiliations**

4 Juan S. Vargas Soto[1,2,*], Rowshyra A. Castañeda[1,2], Nicholas E. Mandrak[1,2] and Péter K. Molnár[1,2]

5 [1] Department of Ecology and Evolutionary Biology, University of Toronto, 25 Willcocks Street, Toronto,

6 Ontario, Canada M5S 3B2

7 [2] Department of Biological Sciences, University of Toronto Scarborough, 1265 Military Trail,

8 Scarborough, Ontario, Canada M1C 1A4

9 * **Corresponding author**: juan.vargassoto@mail.utoronto.ca

10 **Running headline:** Estimating 3D animal density from remote detectors

Abstract

1. Remote detectors are being used increasingly often to study aquatic and aerial species, for which movement is significantly different from terrestrial species. While terrestrial camera-trapping studies have shown that capture frequency, along with the species' movement speed and detector specifications can be used to estimate absolute densities, the approach has not yet been adapted to cases where movement occurs in three dimensions. Frameworks based on animal movement patterns allow estimating population density from camera-trapping data when animals are not individually distinguishable.

2. Here we adapt one such framework to three-dimensional movement to characterize the relationship between population density, animal speed, characteristics of a remote sensor's detection zone, and detection frequency. The derivation involves defining the detection zone mathematically and calculating the mean area of the profile it presents to approaching individuals.

3. We developed two variants of the model – one assuming random movement of all individuals, and one allowing for different probabilities for each approach direction (e.g. that animals more often swim/fly horizontally than vertically). We used computer simulations to evaluate model performance for a wide range of animal and detector densities. Simulations show that in ideal conditions the method approximates true density well, and that estimates become increasingly accurate using more detectors, or sampling for longer. Moreover, the method is robust to invalidation of assumptions, accuracy is decreased only in extreme cases where all detectors are facing the same way.

4. We provide equations for estimating population density from detection frequency and outline how to estimate the necessary parameters. We discuss how environmental variables and species-specific characteristics affect parameter estimates and how to account for these differences in density estimations.

34 5. Our method can be applied to common remote detection methods (cameras and
35 acoustic detectors), which are currently being used to study a diversity of species and environments.
36 Therefore, our work may significantly expand the number and diversity of species for which density can
37 be estimated.

38 **Keywords**

39 3D movement, ideal gas model, population density, population surveys, random encounter model,
40 remote detectors

41

Introduction

Remote detection methods like camera-traps originated for studying surface-dwelling species but are increasingly being used to study aquatic, arboreal, and airborne species. These technologies require considerably less effort and resources than alternatives like transects, particularly for long-term studies, and are less invasive. In aquatic studies, remote underwater video has allowed more efficient, extensive, and less biased sampling than diver-based surveys (King, George, Buckle, Novak, & Fulton, 2018; Mallet & Pelletier, 2014). Similarly, acoustic detectors are becoming a more accessible and popular tool for studying and monitoring a variety of taxa such as birds (Blumstein et al., 2011; Celis-Murillo, Deppe, & Allen, 2009), echolocating bats (Marques et al., 2013), and even fishes that produce species-specific sounds, especially with the aid of automatic identification algorithms (Lindseth, Lobel, Lindseth, & Lobel, 2018). Camera-traps in turn have been useful to study the demographics of elusive species or to learn about biodiversity across different spatial scales (Ahumada et al., 2011; Barea-Azcón, Virgós, Ballesteros-Duperón, Moleón, & Chirosa, 2007; Karanth, Nichols, Kumar, & Hines, 2006). In every case, the technologies, software and analysis methods are constantly evolving (Burton 2015).

Two decades of theoretical developments have created a vast literature of methods for estimating the density of wild populations from camera-trapping data, and some of these methods can be adapted to other types of detectors. Mark-recapture methods, for example, have been used to study aquatic species with individually recognizable spots like whale sharks (*Rhincodon typus*) and eagle rays (Myliobatidae) (González-Ramos, Santos-Moreno, Rosas-Alquicira, & Fuentes-Mascorro, 2017; Meekan et al., 2006). However, most species lack individual markings and are therefore not amenable to these approaches (e.g., Karanth et al. 2006). For these species, existing frameworks for estimating density either provide relative estimates only [e.g. detection frequency, minimum number of detected individuals (Sherman, Chin, Heupel, & Simpfendorfer, 2018), maximum number of conspecifics in a single frame (Willis, Millar, & Babcock, 2000)], or make assumptions about how animals move for

66 estimating absolute density [e.g. movement around a home range centre (Campos-Candela, Palmer,
67 Balle, & Alós, 2018), random walks (Nakashima, Fukasawa, & Samejima, 2018), ideal gas movement
68 (Rowcliffe, Field, Turvey, & Carbone, 2008)]. These movement-based frameworks need to be adapted
69 for key differences between terrestrial and aquatic or aerial species that perceive the world and move in
70 three dimensions.

71 One approach for estimating population density when individuals cannot be distinguished is the
72 Random Encounter Model (REM), formalized for encounters between animals and camera-traps by
73 Rowcliffe et al. (2008). The model assumes that animals move like ideal gases (in straight lines, in
74 random directions, with constant speed) and as a result the frequency at which a species is
75 photographed by camera-traps (henceforth, "detection frequency") scales positively with the number of
76 individuals present in an area (i.e. population density), the species' mean speed, and the size of the
77 camera's detection zone. This relationship can therefore be used to estimate density from the detection
78 frequency. While this method requires more information about a study species than relative abundance
79 measures, it considerably expands the number of species for which density can be estimated using
80 camera-traps. The REM framework can be adapted to species that move in three dimensions rather than
81 two, considering the three-dimensional shape and size of the detection zone.

82 Here, we present such an adaptation to estimate absolute density for aquatic species, using
83 underwater cameras, and for birds and echolocating species, using acoustic sensors. Our adaptation
84 substantially expands possibilities for estimating density from remote detection methods when species
85 can be identified but individuals cannot. This method only requires the detection frequency of a species,
86 information about the sensor's detection zone, and an estimate of the species' speed. We provide two
87 alternatives; the first assumes completely random movement (within the specifications of the ideal gas
88 framework, cf. below), while the second allows accounting for biases in movement direction (e.g. that
89 fish more often swim parallel, rather than perpendicular, to the bottom). First, we will explain the

framework in detail, highlighting the importance of an accurate mathematical description of the detection zone. We will then develop the formulae for density for two types of detectors and test our estimator's performance using computer simulations.

Materials and Methods

1. Model Derivation

1.1. The Random Encounter Model framework

The REM method for estimating density of unmarked animals from camera-trapping data is based on the idea that the encounter rate between a stationary detector and animals of a given species scales linearly with the species' density (see Hutchinson & Waser, 2007), with a scaling factor that depends on the species' movement characteristics and the detector's ability to record animals that are passing by at various distances (Rowcliffe et al., 2008). This relationship is summarized as:

$$D = \frac{f}{\hat{p}\bar{v}} \quad (1)$$

where D is animal density, f is detection frequency, and $\bar{v}$ is mean animal movement speed (See Table 1 for description of parameters). The scaling constant $\hat{p}$ can be thought of as the mean distance (in 2D) or area (in 3D) sampled instantaneously by the detector over all possible directions, and therefore depends on the sensor's technical specifications (opening angles and maximum detection distance) and on environmental variables (e.g. water clarity, foliage or clutter). Here, we will derive an equation for $\hat{p}$ for the three-dimensional case. The main steps are 1) determining the shape of the detection zone, 2) describing it mathematically, and 3) calculating the mean area of its two-dimensional projection. The result is used directly in equation 1 to estimate density from capture frequency. We explain in more detail the projection of the detection zone in Section 2 and derive the density estimator in Section 3. We then test the performance of our estimator with computer-simulated capture data.

Table 1. Parameters used in the derivation of the 3D random encounter method for estimating animal densities.

Parameter	Description
$\hat{p}$	Mean area of the 2D projection of the 3D detection zone.
S, S_i	Surface area of the detection zone, and of its components i.
s	Maximum distance from the detector at which animals can be detected
ϕ	Opening angle of the detector, corresponding to the diagonal field of vision in a camera.
κ, λ, γ	Horizontal, vertical and diagonal fields of vision of a cropped (camera) detector.
μ, ν	Opening angles of the disc sectors that make up the sides of a camera's detection zone
ω, θ	Angles describing the direction of an animal approaching the detection zone, relative to the detector's direction.
D	Population density [animals per unit volume]
$\bar{v}$	Mean movement speed of the study species
f	Detection frequency: the number of independent recordings of a species by a detector, divided by deployment time

1.2. Profile of the detection zone, extension from 2D to 3D

For terrestrial camera-traps, where animals move in two dimensions only, $\hat{p}$ in equation 1 is the mean profile width of the camera's detection zone, as presented to approaching animals. Given the shape of the detection zone, the profile width depends on the direction of approach (Fig. 1). While not explicitly stated by Rowcliffe *et al*. (2008), the "profile" is the projection of the detection zone onto a line perpendicular to the direction of approach. One can therefore use Cauchy's surface area theorem (Cauchy, 1841) to calculate the mean profile width. This theorem states that the average projected area of a convex body is proportional to its surface area. The mean profile width of the two-dimensional detection zone is its perimeter P multiplied by a constant:

$$\hat{p} = \frac{1}{\pi} P \qquad (2)$$

125 which is the same as equation 2 in Rowcliffe et al. (2008). The theorem can readily be applied to

126 determine the mean profile of a three-dimensional detection zone.

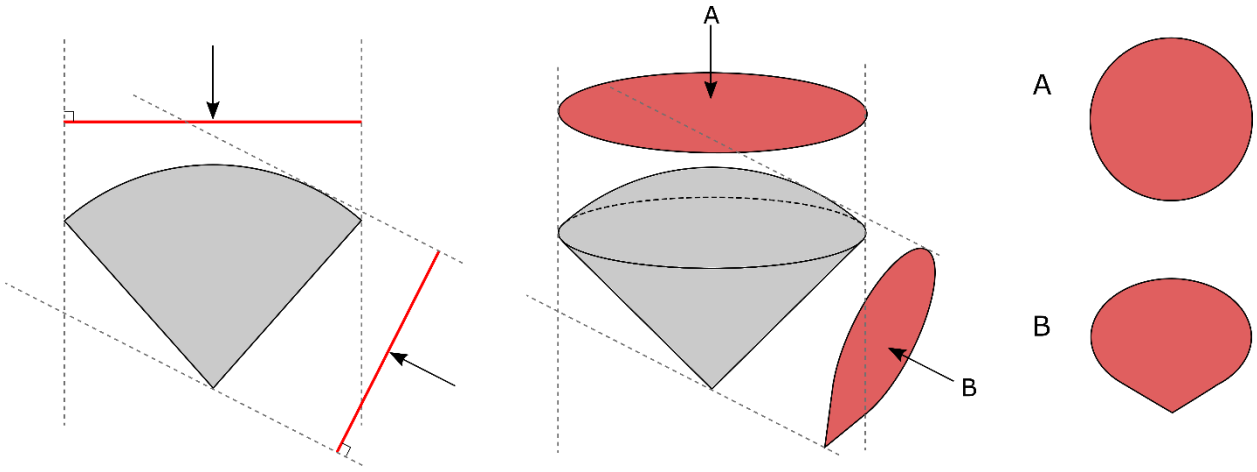

127

128 **Figure 1. The different profiles presented by the detection zone of a remote detector to an approaching animal**

129 **in two (left) or three dimensions (center). In 2D, profiles are lines, while in 3D they are surfaces. The silhouettes**

130 **A and B (right) show the profiles presented to individuals approaching from directions A and B, respectively.**

131

132

133 In the case of a three-dimensional detection zone, equation (1) still holds, with the difference

134 that $\hat{p}$ corresponds to an area instead of a length. This area is nonetheless the projection of the

135 detection zone onto a lower-dimensional object, i.e. onto a plane. According to Cauchy's theorem, the

136 mean projected area of a three-dimensional object is obtained from the surface area *S* as:

137 $$\hat{p} = \frac{1}{4}S \qquad (3)$$

138 (Cauchy, 1841; Vouk, 1948). To calculate S, we will define the detection zone for two types of sensors: a

139 generic sensor with a conical detection zone (acoustic detectors), and the special case of a sensor with a

140 cropped image (i.e. cameras). For acoustic detectors we also determined how to calculate density when

141 there is bias in directions of approach relative to the direction of the detector, for example bats flying
142 most frequently horizontally into a detection zone facing up.

143

144 ## 2. Definition of the detection zone

145 A remote detector's detection zone is generally determined by two parameters: detection angle
146 and maximum distance from which a signal is detectable. Geometrically, this translates into a cone with
147 a convex base. Acoustic detectors report signals no matter where in this zone they occur, but for
148 cameras some near-boundary signals are lost when images are cropped to a rectangular frame. As such,
149 acoustic detectors have the full "conical-with-hat-shaped" detection zone (Fig. 2A), whereas cameras
150 have a subset of this region defined by the horizontal and vertical angles of view (Fig. 2D). In Section 3.1,
151 we derive expressions to calculate the surface area for both detector types and use Cauchy's theorem to
152 calculate the respective mean profile area. This method applies if we assume that all directions of
153 approach are equally likely. In section 3.2, we relax this assumption and consider potential biases in the
154 direction of approach.

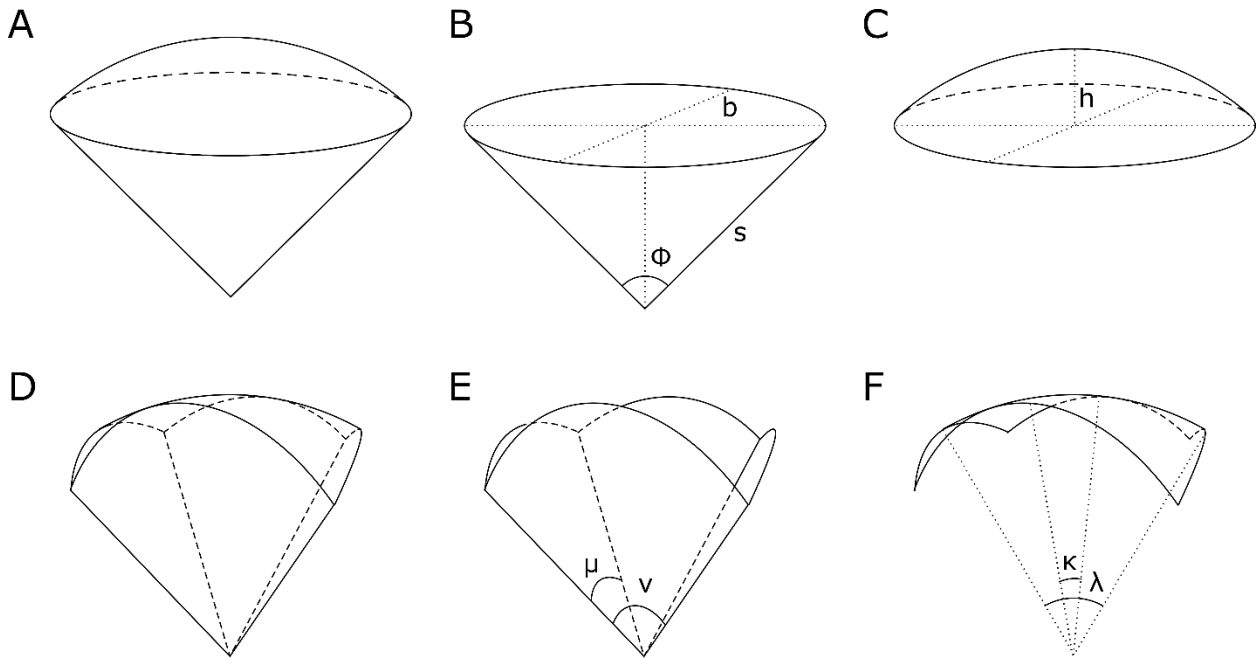

Figure 2. Perspective of the detection zone of (A) an acoustic detector and (D) a camera, where the image is cropped into a rectangle. We decomposed both types of detection zone into bottom and top sections to calculate their surface areas: for acoustic detectors, we considered the lateral surface area S_S of a cone (B), and the area S_C of a spherical cap (C); for cameras, we considered the surface area S_L of four disc segments (E) and the area S_R of a spherical rectangle (F). Parameters are ϕ: opening angle of the detector, *s*: slant height of cone, *b*: basal radius of the cone, *h*: height of the spherical cap, *μ* and *ν*: angles of the disc segments that make up the sides of the cropped detection zone, *κ* and *λ*: horizontal and vertical fields of vision of the camera

2.1. Uniformly distributed approach directions

To calculate the surface area of an acoustic sensor's detection zone, we divide the detection zone into two components: a conic base (Fig. 2B) and a spherical cap (Fig. 2C). The lateral surface area of the cone is calculated from the slant height, *s* (i.e. the maximum detection distance), and the cone's basal radius, *b*, as:

169
$$S_C = \pi bs$$
$$S_C = \pi s^2 \sin\frac{\phi}{2} \quad (4)$$

170 where ϕ is the detector's opening angle. The spherical cap's surface area is $S_S = 2\pi sh$ (Kern & Bland,

171 1938), where *h* is the cap's height, given by $h = s(1 - \cos\frac{\phi}{2})$ (Appendix A1), so:

172
$$S_S = 2\pi s^2 \left(1 - \cos\frac{\phi}{2}\right) \quad (5)$$

173 Combining equations (4) – (5), we obtain the mean profile area of an acoustic detector's detection zone:

174
$$\widehat{p_{ad}} = \frac{1}{4}(S_C + S_S)$$

175
$$\widehat{p_{ad}} = \frac{1}{4}\left(\pi s^2 \sin\frac{\phi}{2} + 2\pi s^2 \left(1 - \cos\frac{\phi}{2}\right)\right)$$

176
$$\widehat{p_{ad}} = \frac{1}{4}\pi s^2 \left(2 - 2\cos\frac{\phi}{2} + \sin\frac{\phi}{2}\right) \quad (6)$$

177 Cauchy's theorem is only valid for convex bodies, so equation 6 only applies when the detection

178 angle is smaller than π (180°) or equal to 2π (360°). The latter occurs when signals can be detected from

179 any direction, as is the case with omnidirectional microphones. Consider for example an acoustic

180 detector with a detection angle of 90° (π/2 rad) that can detect signals from 10 meters away.

181 Substituting *s* and ϕ in eq. 6 we obtain:

182
$$\widehat{p_{ad}} = \frac{1}{4}\pi \times 10^2 \left(2 - 2\cos\left(\frac{1}{2} \times \frac{\pi}{2}\right) + \sin\left(\frac{1}{2} \times \frac{\pi}{2}\right)\right)$$

183
$$\widehat{p_{ad}} = 101.5\ m^2$$

184 To calculate the surface area of a camera's detection zone, we note that image cropping creates

185 a detection zone bounded by a spherical rectangle cap sitting atop two pairs of disc sectors of radius *s*

186 and delimited by angles μ and ν (Fig. 2D). These angles are related to the vertical (λ), horizontal (κ), and

187 diagonal (γ) fields of vision of the camera, of which at least one is normally provided by the

188 manufacturer (see Appendix A3 for how to calculate the unknown angles). As the surface areas of the

189 disc sectors are given by $S_\nu = \pi s^2 \frac{\nu}{2\pi}$ or $S_\mu = \pi s^2 \frac{\mu}{2\pi}$, respectively, the total lateral surface area of the

190 camera's detection zone, S_L (Fig. 1E), becomes

191 $$S_L = 2S_\nu + 2S_\mu = s^2(\mu + \nu) \tag{7}$$

192 Furthermore, the surface area of the spherical rectangle cap, S_R (Fig. 1F), is obtained by multiplying the

193 surface area of a sphere of radius *s* by the proportion of the sphere occupied by the spherical rectangle:

194 $$S_R = 4\pi s^2 \frac{\Omega}{4\pi}$$

195 $$= s^2\Omega \tag{8}$$

196 where Ω is the solid angle delimited by the horizontal and vertical fields of vision, κ and λ, given by

197 (Appendix A2):

198 $$\Omega = 4 \arcsin \frac{\tan\frac{\kappa}{2}\tan\frac{\lambda}{2}}{\sqrt{1+\tan^2\frac{\kappa}{2}}\sqrt{1+\tan^2\frac{\lambda}{2}}} \tag{9}$$

199 The mean profile area for a camera is therefore:

$$\widehat{p_{cam}} = \frac{1}{4}(S_L + S_R)$$

200 $$\widehat{p_{cam}} = \frac{1}{4}\left(s^2(\mu+\nu) + 4s^2 \arcsin \frac{\tan\frac{\kappa}{2}\tan\frac{\lambda}{2}}{\sqrt{1+\tan^2\frac{\kappa}{2}}\sqrt{1+\tan^2\frac{\lambda}{2}}} \right)$$

$$\widehat{p_{cam}} = \frac{1}{4}s^2\left(\mu+\nu+4 \arcsin \frac{\tan\frac{\kappa}{2}\tan\frac{\lambda}{2}}{\sqrt{1+\tan^2\frac{\kappa}{2}}\sqrt{1+\tan^2\frac{\lambda}{2}}} \right) \tag{10}$$

201 Consider for example an underwater camera with horizontal and vertical fields of vision (FOV) of

202 122.6° (2.1 rad) and 94.4° (1.6 rad), respectively (these correspond to a GoPro Hero 7 using a wide 4:3

aspect ratio). Using eq. S3.2 we obtain a diagonal FOV of 154.5° (2.7 rad) and using eq. S3.4 we obtain the lateral angles μ = 142.1° = 2.5 rad and v = 125.2° = 2.2 rad. Substituting these values in eq. 10, assuming again a detection distance of 10 m, we obtain the mean profile area for this camera:

$$\widehat{p_{cam}} = \frac{1}{4} \times 10^2 \left(2.5 + 2.2 + 4 \arcsin \frac{\tan\frac{2.1}{2} \tan\frac{1.6}{2}}{\sqrt{1+\tan^2\frac{2.1}{2}}\sqrt{1+\tan^2\frac{1.6}{2}}} \right)$$

$$\widehat{p_{cam}} = 186.6\ m^2$$

2.2. Bias in direction of movement

The method described above for calculating the detection zone's mean profile area $\hat{p}$ assumes that every direction of approach is equally likely. However, some angles of approach could occur more frequently than others depending both on the study species and the placement and orientation of the detector. Picture, for example, fish moving in a stream in the direction of the current. The profile presented to all of them by a camera is the same and the effective mean profile area is greater or lower than the expected mean profile area, depending on which way the detector is facing. To account for these biases, we derive formulae to calculate the detection zone's projected area p for any direction of approach and then weight these according to the probability of approach directions. As these calculations quickly become lengthy and complicated, we here summarize the approach for acoustic detectors and provide detailed calculations in Appendix A4.

The mean profile area is given by:

$$\hat{p} = \frac{1}{\pi} \int_0^{\pi} P(\omega) p(\omega)\, d\omega \qquad (11)$$

where *P(ω)* is the probability that an individual approaches the detector at angle ω, and *p(ω)* gives the profile area corresponding to that direction. Depending on ω – the angle relative to the direction of the

223 detector – the different components of the detection zone may be visible or hidden. We obtain

224 therefore four different formulae to calculate *p(ω)*:

225
$$p(\omega) = \begin{cases} a_e, & \sin\omega \le \sin\frac{\phi}{2} \; and \; \sin\omega \le \cos\frac{\phi}{2} \\ a_e + a_d, & \sin\omega \le \sin\frac{\phi}{2} \; and \; \sin\omega > \cos\frac{\phi}{2} \\ a_e + a_h, & \sin\omega > \sin\frac{\phi}{2} \; and \; \sin\omega \le \cos\frac{\phi}{2} \\ a_e + a_d + a_h, & \sin\omega > \sin\frac{\phi}{2} \; and \; \sin\omega > \cos\frac{\phi}{2} \end{cases} \quad (12)$$

226 The first element, a_e, corresponds to the area of the projection encompassed by the base of the cone

227 (area I in Fig. 3), while the areas a_h and a_d are the projections of the visible parts of the spherical cap

228 (area II) and the cone (area III). The derivation of a_e, a_h, a_d, and the rationale behind them are given in

229 Appendix A4.

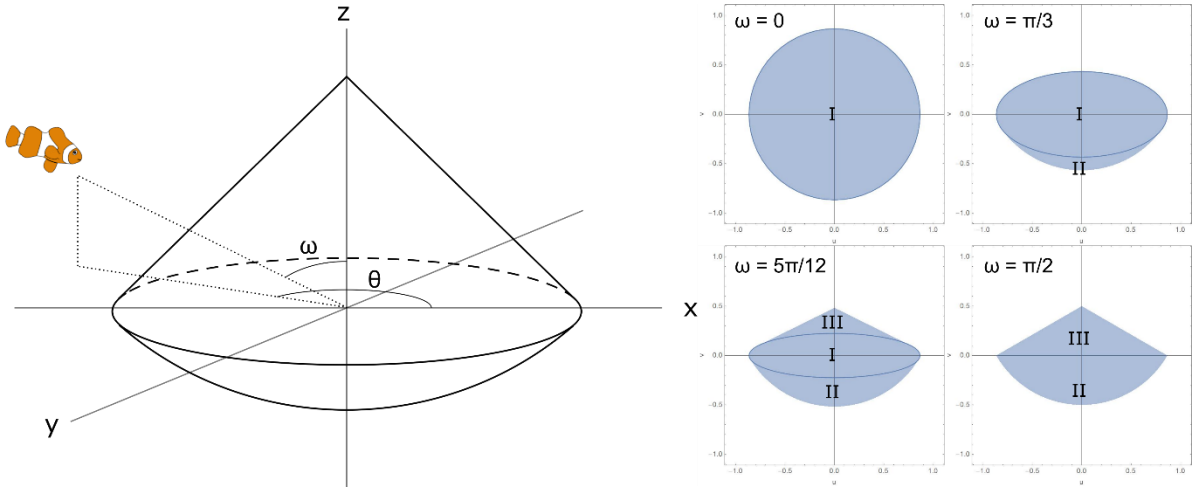

230

231 **Figure 3. Perspective of a conic detection zone (left), showing the angles ω and θ that define the direction of**

232 **approach of an individual. Different angles ω result in different profiles (right). The labels indicate the different**

233 **areas that need to be calculated in each case; I is the area of the projection encompassed by the circle at the**

234 **base of the cone, II is the projection of the spherical cap, III is the projection of the cone's sides.**

235

3. Simulation tests

We tested the formula for estimating density from detection frequency using computer simulations. Firstly, these serve to confirm that the method performs well under ideal conditions (i.e. when all model assumptions are met and perfect information about the species' movement is available) and secondly to test the robustness to invalidation of assumptions. The assumptions regarding animal movement are those of the ideal gas model: individuals moving in a straight line, in random directions, and at a constant speed. We assumed perfect detection and an exact knowledge of the detection distance and opening angle and evaluated the method's performance for a range of animal densities and detector numbers. Furthermore, to determine the robustness of our method, we evaluated its performance for the following scenarios: (i) allowing variation in speed by randomly selecting different individual speeds; (ii) allowing a non-random distribution of approach directions by randomly selecting individual 'tilt' angles, combined with realistic scenarios of detector placement and orientation.

We set up the simulation as follows: Individuals were distributed at random locations within a cube of side 10, and each one was assigned a random direction (x, y, z vector components drawn from a uniform distribution from -1 to 1). All individuals moved at the same speed and bounced back into the cube if they reached the reflective boundaries. We tested the density estimator for a range of densities between 0.1 and 10 ind.uv^{-1} (individuals per unit volume), i.e. between 100 and 10000 individuals.

We placed between 5 and 25 detectors facing in random directions at random locations within the 'sampling zone', a cube of side 4 situated at the centre of the larger cube. We set a detection distance of 0.5 ud (unit distance) and a detection angle of 45°, which yields a mean profile area of 0.105 ua (unit area) (equation 6).

We set movement speed equal to one length of the detection radius per time step and ran each simulation for 40 steps. We counted an encounter whenever an individual entered a detection zone.

Thus, we obtained for each step and each detector the total number of detections up to that time point. We calculated the detection frequency f by dividing this cumulative count by the number of steps and then divided f by the mean profile area and the movement speed to estimate density (eq. 1). We recorded the mean estimated density across all detectors at every time step. We also determined how performance changed with effort both in terms of the number of detectors and sampling time.

To test how variability in speed among individuals affected density estimates, we ran simulations assigning each individual a speed drawn at random from a normal distribution with mean 0.5 ud/step, and with standard deviation between 0 and 0.1 ud/step. Similarly, to determine the effect of having biased movement directions, we drew the vertical (z) component of the individual direction vectors from a truncated normal distribution centred around 0 and bounded between -1 and 1, so that most individuals would move near horizontally. We assessed the effect of this bias on the performance of the estimator for several scenarios of detector distribution (regular spacing of detectors in 2D on a plane, regular spacing in 3D throughout the sampling cube, random distribution in 3D) and orientation (all horizontal, all vertical, random). These simulations were run with ten detectors.

We iterated each scenario 100 times, and assessed model performance by calculating the bias, precision and accuracy of the density estimate relative to the real density at the end of each simulation. We used the scaled mean error (SME), the coefficient of variation (CV) and the scaled mean square error (SMSE) as indicators of bias, precision, and accuracy, respectively:

$$SME = \frac{1}{An}\sum_{j=1}^{n}\left(E_j - A\right)$$

$$CV = \frac{SD}{\bar{E}}$$

$$SMSE = \frac{1}{A^2 n}\sum_{j=1}^{n}\left(E_j - A\right)^2$$

where $\bar{E}$ is the mean density estimate, E_j is the density estimate of the j^{th} iteration, SD is the standard deviation of density estimates across iterations, A is the real density, and n is the number of iterations (Walther & Moore, 2005). The bias metric SME indicates whether the true value is over- or underestimated, the precision metric CV indicates the variability among estimates, and the accuracy metric SMSE measures both bias and precision in a single index. The closer to zero each index is, the better the performance of the estimator.

Results

Simulations show that, under ideal conditions, the estimated density closely approximates the real density. Regardless of the number of detectors used, the estimate density was within 5% of the real value at the end of each simulation (Fig. 4A), and the standard deviation was no larger than 30% of the mean estimate (Fig. 4B). The overall performance of the method nonetheless depended on sampling effort, both in terms of the number of detectors and the sampling time. The lowest number of detectors yielded the greatest bias and the lowest precision and accuracy, and all indices improved substantially with the deployment of additional detectors (Fig. 4A-C). Moreover, bias also decreases, and precision and accuracy increase, as sampling time increases (Fig. 4D-F), meaning that in real-life applications a low availability of detectors could at least be partially compensated for by longer sampling times.

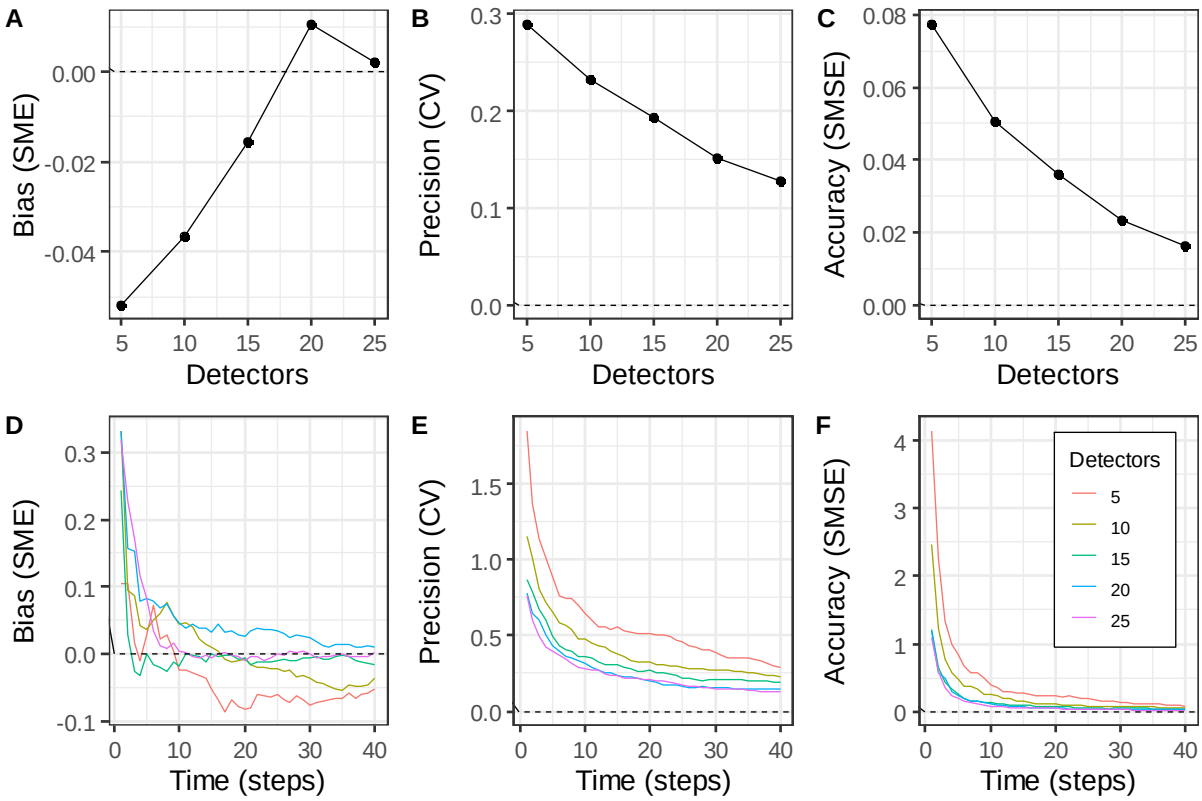

297

298 **Figure 4. Performance of the 3D density estimation method for different levels of effort. The top row shows the**
299 **mean bias, precision, and accuracy metric values at the end of the simulations as a function of the number of**
300 **detectors deployed. The bottom row shows the change in these metrics as time progresses in the simulation.**

301

302 The real density did not seem to bias the estimator, except at extremely low densities (Fig. 5A). Precision
303 (Fig. 5B), and thus overall accuracy (Fig. 5C), however, depended strongly on the population's density,
304 with the estimator's CV decreasing by a factor of more than 9 between the lowest (0.1 ind.uv^{-1}) and

highest (10 ind.uv^{-1}) densities considered.

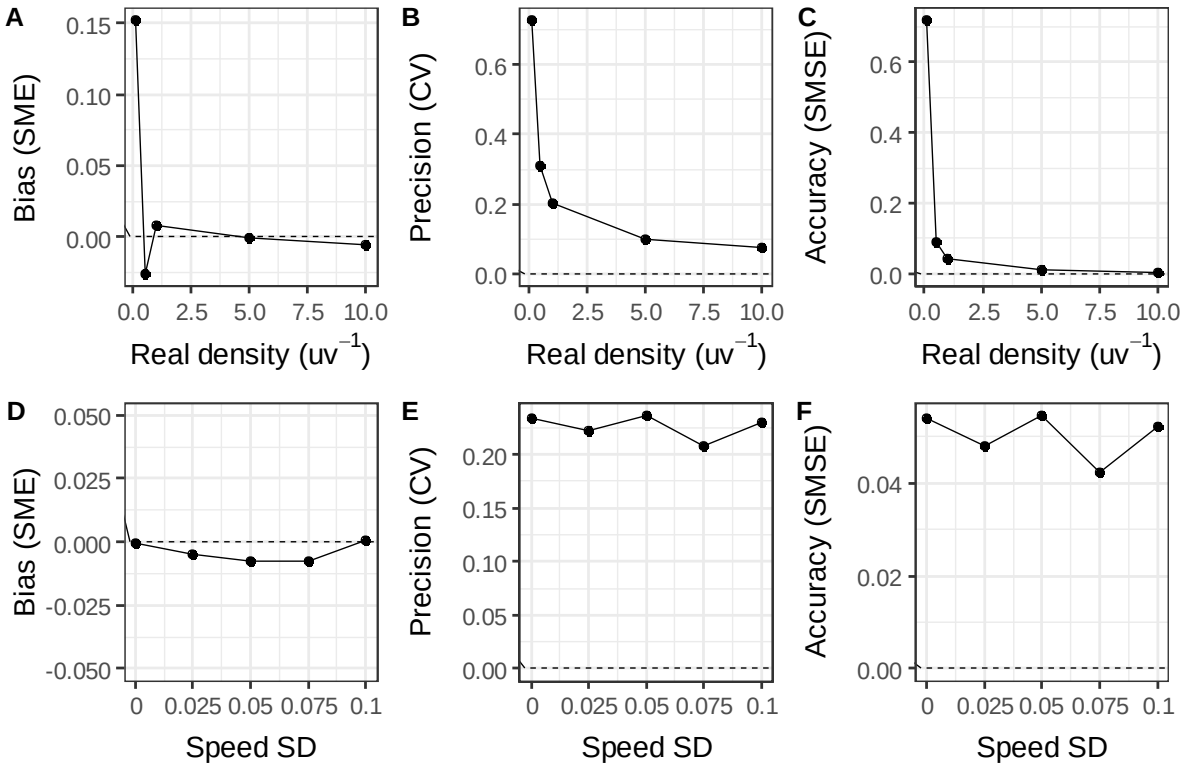

Figure 5. Effects of population density (top row), and among-individual variability in movement speed (bottom row) on the performance of the 3D density estimation method. All parameters were as described in the text, using in particular a constant mean speed of 0.5 ud/step in the top row, and varying the speed among individuals by drawing from a normal distribution with standard deviation between 0 and 0.1 ud in the bottom row.

The simplifying assumption of equal movement speeds among individuals appears to be robust, as introducing among-individual variance in speed did not noticeably affect the estimator's bias, precision, or accuracy (Figs. 5D-F).

Having biases in the direction of movement, however, did decrease performance in some scenarios, particularly when all individuals were moving horizontally, i.e. with a standard deviation of zero around

the mean direction. In this case, precision and accuracy decreased when detectors were placed on a single plane and oriented vertically (Fig. 6D, G) or horizontally (Fig. 6E, H). Conversely, detectors distributed regularly or randomly across the 3D space yielded similar accuracy and precision estimates for all cases of movement direction bias. Nevertheless, there was virtually equal performance regardless of detector placement when detectors faced in random directions (Fig. 6F, I). Moreover, the random orientation of detectors also generally lowered the estimator's bias compared to the scenarios where all detectors were facing vertically or horizontally (contrast Figs. 6A-C).

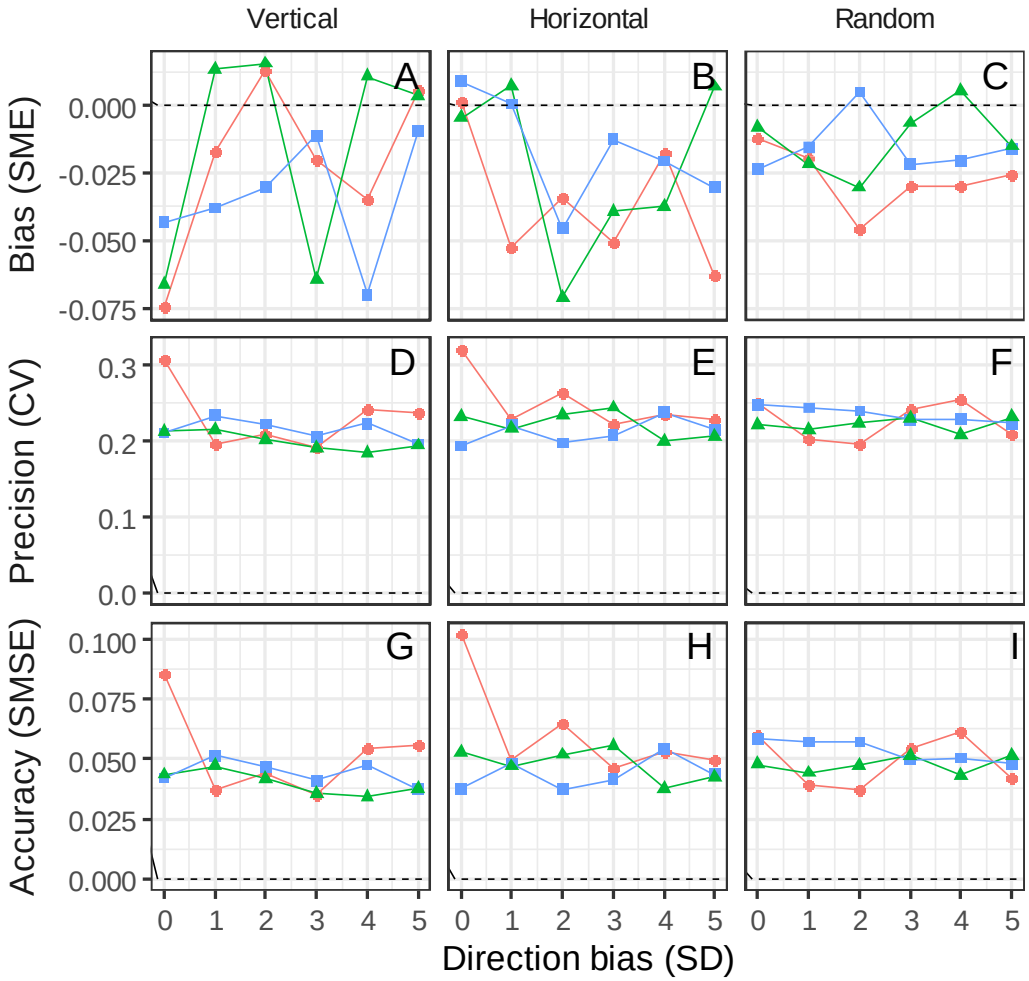

Figure 6. Effects of sampling strategies and animal movement bias on the performance of the 3D density estimation method. Columns represent the orientation of detectors: all vertical (left), all horizontal

(middle) or all random (right). Symbols show the distribution of detectors: regular spacing on a 2D plane (circles), regular spacing in 3D throughout the sampling cube (triangles), and random distribution in 3D (squares). Parameters are as described in the text, using in particular a vertical direction component drawn at random from a truncated normal distribution centred at 0 with standard deviations between 0 and 5 to show direction bias.

Discussion

We have outlined a method to use remote detectors such as underwater cameras or acoustic sensors to estimate population density from an encounter rate. The underlying random encounter model was originally proposed and tested as a density estimator for species moving in a two-dimensional terrestrial environment by Rowcliffe et al. (2008), and our calculations now allow its adaptation to species that move in three dimensions such as fishes, birds and bats. The basic requirements regarding detector specifications and information on movement speed remain the same as for the two-dimensional case.

Simulations show good performance of the estimator, low levels of bias, and a high degree of precision. Such consistent performance was expected when all assumptions were met, which may not be the case in real-life applications. We showed, however, that the method is robust to violations of assumptions. There was very little effect of increased variance in speed among individuals, or of bias in direction. Furthermore, our simulation results suggest that any effect could be limited or altogether eliminated simply by orienting detectors in different directions, even when detectors are placed on a single plane (on the ground, for example).

Performance is significantly influenced by sampling effort as it relates to the real density, in terms of both time and number of detectors. At low densities especially, insufficient effort could result

in an over- or underestimation of density. An advantage of using a method based on movement models is that researchers can use the same framework to calculate the effort needed beforehand. Rearranging eq. 1 and substituting density and speed with prior information allows calculating an expected capture frequency. We saw no bias at higher densities, but we expect that in practice extremely high densities (e.g. in fish schools) may prevent properly counting individuals, resulting in underestimated densities. In these cases, researchers could first estimate a density of groups and obtain overall density by multiplying this estimate by an independently calculated mean group size (Rowcliffe et al. 2008).

Our method can be applied in cases where a lack of individual markings impedes the use of mark-recapture techniques. It is also an improvement over indices of relative abundance such as the maximum or mean number of conspecifics in a single frame (Schobernd, Bacheler, & Conn, 2014; Sherman et al., 2018). These metrics are commonly used to analyse footage from baited-remote-underwater-video-stations (BRUVS), but can underestimate true abundance (Cappo, Harvey, Malcolm, & Speare, 2003; Stobart et al., 2015). We know of no similar tools to estimate abundance from acoustic detectors. These sensors allow to identify species and count passages through the detection zone, so our method is also applicable with these technologies, provided the detection zone and mean species speed can be accurately measured.

For many species, mean speed will not be immediately available in the literature but could be approximated with additional measurements. For example, using two cameras in a stereo arrangement, the footage from both could be used to estimate speed (Somerton, Williams, & Campbell, 2017; Williams, Rooper, & Towler, 2010) and – using only one of the two cameras – population density in the same study.. Movement If detectors are deployed for several days the estimation of mean speed must include periods of inactivity (see Carbone, Cowlishaw, Isaac, & Rowcliffe, 2005). Ideally, surveys should be conducted at the same time of day when working in different sites, during the species' daily activity peak.

375 Additional to speed, an exact characterization of the detection zone is required to estimate
376 density accurately. This zone is determined first by the opening angle (for acoustic detectors), or the
377 horizontal and vertical fields of vision (for cameras), usually given by the manufacturer. However, action
378 cameras commonly used in remote underwater surveys have wide-angle lenses, which distort the
379 image. Because of this, the diagonal field of vision will not correspond to the angle calculated assuming
380 a rectilinear lens (see Appendix A3). The additional area in the projection due to the distortion should be
381 small, so we suggest assuming a rectilinear lens for consistency.

382 The second element needed to characterize the detection zone is the detection radius. Unlike
383 the opening angles the detection radius is influenced by environmental variables. For example, for
384 underwater cameras, detection distance depends on visibility (i.e. turbidity), which should be
385 considered when comparing densities across sites. Similarly, for acoustic detectors, atmospheric
386 conditions like temperature and humidity affect how far an acoustic signal travels, effectively influencing
387 the detection distance for birds and bats (Lawrence & Simmons, 1982; Snell-Rood, 2012). In both
388 aquatic and aerial surveys, physical obstacles such as vegetation will also limit detectability; for instance,
389 detection of bats with low-frequency calls (25 kHz) is significantly hindered by habitat structure
390 (Patriquin, Hogberg, Chruszcz, Barclay, & Barclay, 2003; Weller & Zabel, 2002).

391 Environmental variables also interact with species-specific traits, generating different detection
392 distances even under comparable environmental conditions. For example, cameras can detect larger
393 species further than smaller species, and acoustic detectors will detect species with lower frequency or
394 more intense calls at greater distances from than species with high-frequency calls (Jakobsen, Brinkløv,
395 & Surlykke, 2013; Lawrence & Simmons, 1982; Snell-Rood, 2012; Surlykke & Kalko, 2008). Given the
396 multiple factors that influence detection distance, we suggest an ad-hoc calculation for every system, for
397 example placing a model of the study species progressively further from a camera until it is no longer
398 recognizable. With acoustic detectors the same can be done using a speaker at a range of distances.

399 Our calculations are performed for individual detectors, but, as our simulations show, the best
400 results are obtained when averaging across multiple detectors. Improved performance using more
401 detectors is to be expected, as averaging across detectors minimizes possible sampling errors (Rowcliffe
402 et al., 2008). Using more detectors also reduced variability across trials, implying that less effort is
403 required to obtain accurate density estimates. Sampling designs should seek to maximize the number of
404 encounters with a target species. using a number and spacing of detectors that capture the movement
405 of the species of interest, while maintaining independence across detectors (Keiter et al., 2017).

406 Finally, we note that detection zones can also be affected by placement. Cameras placed in
407 shallow streams, for example, could have their detection zone cut at the top by the surface and at the
408 bottom by the substrate. In these cases, the resulting video frames can be cropped so that neither the
409 ground nor the surface are visible, and the fields of vision and capture frequency recalculated
410 accordingly (this would be equivalent to having a camera with narrower field of vision). If topography
411 permits, one can prevent the issue of an incomplete detection zone by placing the camera in mid-water
412 such that neither the water surface nor the bottom are visible. This would be a departure from current
413 designs that set cameras on the ground but would avoid the issue of cropping the detection zone. For
414 benthic species or very shallow streams none of these solutions might be feasible, and we would
415 recommend using a 2D approach.

416 In summary, we have proposed a method for estimating density in three dimensions using data
417 from remote detectors, which can be used in ecological and conservation research and as a monitoring
418 tool. The description of detection zones provided will be useful in translating other density estimation
419 methods that are also based on the ideal gas model (Campos-Candela et al., 2018; Moeller, Lukacs, &
420 Horne, 2018). There is an extensive and growing literature characterizing sampling requirements for
421 camera-traps in two dimensions, but such considerations are practically non-existent for species moving
422 in three dimensions (Burton et al., 2015; O'Connell, Nichols, & Karanth, 2010). Our analyses allow

423 extending these considerations to three dimensions, and it is our hope that our work will prompt new
424 study designs and applications of remote detection methods to study a broader range of species and
425 environments. We lay out the theoretical foundation of the method but recognize that it will require
426 empirical validation. The sampling of aquatic, airborne, and arboreal species each comes with intrinsic
427 challenges and field trials must be conducted to confirm that the method performs in real conditions as
428 well as predicted by simulations. Given the existing camera-trapping literature and the use of
429 underwater cameras to estimate abundance, we believe the application of our method will be more
430 straightforward in underwater censuses. The application to acoustic detectors will require further work
431 to characterize the detection zone, as currently there is no quantitative way to measure the detection
432 distance under different environmental conditions. Thus, the requirements of our method open new
433 avenues of research in remote detection.

Acknowledgments

PKM is grateful for support from an NSERC (Natural Sciences and Engineering Research Council of Canada) Discovery Grant, CFI (Canada Foundation for Innovation) John R. Evans Leader Funds, and MRIS Ontario Research Funds. Funding by FRQNT (Fonds de recherche nature et technologie) to RAC and an NSERC Discovery Grant to NEM is gratefully acknowledged.

Authors' contributions

RAC, PKM and JSVS conceived the original concept. JSVS and PKM derived the equations. JSVS conducted simulations and led the writing of the manuscript. All authors contributed critically to the drafts and gave final approval for publication.

Data accessibility

The code for the simulations and to reproduce figures is available on github in the following repository: juansvs/3D_DensityEstimation

447 **References**

448 Ahumada, J. A., Silva, C. E. F., Gajapersad, K., Hallam, C., Hurtado, J., Martin, E., … Andelman, S. J. (2011).
449 Community structure and diversity of tropical forest mammals: data from a global camera trap
450 network. *Philosophical Transactions of the Royal Society of London. Series B, Biological Sciences*,
451 *366*(1578), 2703–11. doi:10.1098/rstb.2011.0115

452 Barea-Azcón, J. M., Virgós, E., Ballesteros-Duperón, E., Moleón, M., & Chirosa, M. (2007). Surveying
453 carnivores at large spatial scales: a comparison of four broad-applied methods. *Biodiversity and*
454 *Conservation*, *16*(4), 1213–1230. doi:10.1007/s10531-006-9114-x

455 Blumstein, D. T., Mennill, D. J., Clemins, P., Girod, L., Yao, K., Patricelli, G., … Kirschel, A. N. G. (2011).
456 Acoustic monitoring in terrestrial environments using microphone arrays: applications,
457 technological considerations and prospectus. *Journal of Applied Ecology*, *48*, 758–767.
458 doi:10.1111/j.1365-2664.2011.01993.x

459 Burton, A. C., Neilson, E., Moreira, D., Ladle, A., Steenweg, R., Fisher, J. T., … Boutin, S. (2015). REVIEW:
460 Wildlife camera trapping: a review and recommendations for linking surveys to ecological
461 processes. *Journal of Applied Ecology*, *52*(3), 675–685. doi:10.1111/1365-2664.12432

462 Campos-Candela, A., Palmer, M., Balle, S., & Alós, J. (2018). A camera-based method for estimating
463 absolute density in animals displaying home range behaviour. *Journal of Animal Ecology*, *87*(3),
464 825–837. doi:10.1111/1365-2656.12787

465 Cappo, M., Harvey, E., Malcolm, H., & Speare, P. (2003). Potential of video techniques to monitor
466 diversity, abundance and size of fish in studies of marine protected areas. University of
467 Queensland.

468 Carbone, C., Cowlishaw, G., Isaac, N. J. B., & Rowcliffe, J. M. (2005). How Far Do Animals Go?

469 Determinants of Day Range in Mammals. *The American Naturalist*, *165*(2), 290–297.
470 doi:10.1086/426790

471 Cauchy, A. (1841). Note sur divers théorèmes relatifs à la rectification des courbes et à la quadrature des
472 surfaces. *Comptes Rendus de l'Académie de Sciences*, *13*, 1060–1065.

473 Celis-Murillo, A., Deppe, J. L., & Allen, M. F. (2009). Using soundscape recordings to estimate bird
474 species abundance, richness, and composition. *Journal of Field Ornithology*, *80*(1), 64–78.
475 doi:10.1111/j.1557-9263.2009.00206.x

476 González-Ramos, M. S., Santos-Moreno, A., Rosas-Alquicira, E. F., & Fuentes-Mascorro, G. (2017).
477 Validation of photo-identification as a mark-recapture method in the spotted eagle ray *Aetobatus*
478 *narinari*. *Journal of Fish Biology*, *90*(3), 1021–1030. doi:10.1111/jfb.13215

479 Hutchinson, J. M. C., & Waser, P. M. (2007). Use, misuse and extensions of "ideal gas" models of animal
480 encounter. *Biological Reviews*, *82*(3), 335–359. doi:10.1111/j.1469-185X.2007.00014.x

481 Jakobsen, L., Brinkløv, S., & Surlykke, A. (2013). Intensity and directionality of bat echolocation signals.
482 *Frontiers in Physiology*, *4*, 89. doi:10.3389/fphys.2013.00089

483 Karanth, K. U., Nichols, J. D., Kumar, S., & Hines, J. E. (2006). Assessing Tiger Population Dynamics Using
484 Photographic Capture – Recapture Sampling. *Ecology*, *87*(11), 2925–2937. doi:10.1890/0012-
485 9623(2006)87[323:ATPD]2.0.CO;2

486 Keiter, D. A., Davis, A. J., Rhodes, O. E., Cunningham, F. L., Kilgo, J. C., Pepin, K. M., & Beasley, J. C.
487 (2017). Effects of scale of movement, detection probability, and true population density on
488 common methods of estimating population density. *Scientific Reports*, *7*(1), 9446.
489 doi:10.1038/s41598-017-09746-5

490 Kern, W. F., & Bland, J. R. (1938). *Solid mensuration with proofs* (2nd ed.). London: Chapman & Hall.

King, A. J., George, A., Buckle, D. J., Novak, P. A., & Fulton, C. J. (2018). Efficacy of remote underwater video cameras for monitoring tropical wetland fishes. *Hydrobiologia*, *807*(1), 145–164. doi:10.1007/s10750-017-3390-1

Lawrence, B. D., & Simmons, J. A. (1982). Measurements of atmospheric attenuation at ultrasonic frequencies and the significance for echolocation by bats. *The Journal of the Acoustical Society of America*, *71*(3), 585–590. doi:10.1121/1.387529

Lindseth, A., Lobel, P., Lindseth, A. V., & Lobel, P. S. (2018). Underwater Soundscape Monitoring and Fish Bioacoustics: A Review. *Fishes*, *3*(3), 36. doi:10.3390/fishes3030036

Mallet, D., & Pelletier, D. (2014). Underwater video techniques for observing coastal marine biodiversity: A review of sixty years of publications (1952–2012). *Fisheries Research*, *154*, 44–62. doi:10.1016/j.fishres.2014.01.019

Marques, T. A., Thomas, L., Martin, S. W., Mellinger, D. K., Ward, J. A., Moretti, D. J., … Tyack, P. L. (2013). Estimating animal population density using passive acoustics. *Biological Reviews*, *88*(2), 287–309. doi:10.1111/brv.12001

Meekan, M. G., Bradshaw, C. J. A., Press, M., McLean, C., Richards, A., & Quasnichka, S. (2006). Population size and structure of whale sharks Rhincodon typus at Ningaloo Reef, Western Australia . *Marine Ecology Progress Series*, *319*, 275–285.

Moeller, A. K., Lukacs, P. M., & Horne, J. S. (2018). Three novel methods to estimate abundance of unmarked animals using remote cameras. *Ecosphere*, *9*(8), e02331. doi:10.1002/ecs2.2331

Nakashima, Y., Fukasawa, K., & Samejima, H. (2018). Estimating animal density without individual recognition using information derivable exclusively from camera traps. *Journal of Applied Ecology*, *55*(2), 735–744. doi:10.1111/1365-2664.13059

513 O'Connell, A., Nichols, J., & Karanth, K. (2010). *Camera traps in animal ecology: methods and analyses*.

514 Patriquin, K. J., Hogberg, L. K., Chruszcz, B. J., Barclay, R. M. R., & Barclay, R. M. B. (2003). The influence
515 of habitat structure on the ability to detect ultrasound using bat detectors. *Wildlife Society Bulletin*,
516 *31*(2), 475–481.

517 Rowcliffe, J. M., Field, J., Turvey, S. T., & Carbone, C. (2008). Estimating animal density using camera
518 traps without the need for individual recognition. *Journal of Applied Ecology*, *45*(4), 1228–1236.
519 doi:10.1111/j.1365-2664.2008.01473.x

520 Schobernd, Z. H., Bacheler, N. M., & Conn, P. B. (2014). Examining the utility of alternative video
521 monitoring metrics for indexing reef fish abundance. *Canadian Journal of Fisheries and Aquatic*
522 *Sciences*, *71*(3), 464–471. doi:10.1139/cjfas-2013-0086

523 Sherman, C. S., Chin, A., Heupel, M. R., & Simpfendorfer, C. A. (2018). Are we underestimating
524 elasmobranch abundances on baited remote underwater video systems (BRUVS) using traditional
525 metrics? *Journal of Experimental Marine Biology and Ecology*, *503*, 80–85.
526 doi:10.1016/J.JEMBE.2018.03.002

527 Snell-Rood, E. C. (2012). The effect of climate on acoustic signals: Does atmospheric sound absorption
528 matter for bird song and bat echolocation? *The Journal of the Acoustical Society of America*,
529 *131*(2), 1650–1658. doi:10.1121/1.3672695

530 Somerton, D. A., Williams, K., & Campbell, M. D. (2017). Quantifying the behavior of fish in response to a
531 moving camera vehicle by using benthic stereo cameras and target tracking. *Fishery Bulletin*,
532 *115*(3), 343–354. doi:10.7755/FB.115.3.5

533 Stobart, B., Díaz, D., Álvarez, F., Alonso, C., Mallol, S., & Goñi, R. (2015). Performance of Baited
534 Underwater Video: Does It Underestimate Abundance at High Population Densities? *PLOS ONE*,

10(5), e0127559. doi:10.1371/journal.pone.0127559

Surlykke, A., & Kalko, E. K. V. (2008). Echolocating Bats Cry Out Loud to Detect Their Prey. *PLoS ONE*, *3*(4), e2036. doi:10.1371/journal.pone.0002036

Vouk, V. (1948). Projected area of convex bodies. *Nature*, *162*, 330–331. doi:10.1038/162330a0

Walther, B. A., & Moore, J. L. (2005). The concepts of bias, precision and accuracy, and their use in testing the performance of species richness estimators, with a literature review of estimator performance. *Ecography*, *28*(6), 815–829. doi:10.1111/j.2005.0906-7590.04112.x

Weller, T. J., & Zabel, C. J. (2002). Variation in bat detections due to detector orientation in a forest. *Wildlife Society Bulletin*, *30*(3), 922–930.

Williams, K., Rooper, C. N., & Towler, R. (2010). Use of stereo camera systems for assessment of rockfish abundancein untrawlable areas and for recording pollock behavior during midwater trawls. *Fishery Bulletin*, *108*(3), 352–362.

Willis, T., Millar, R., & Babcock, R. (2000). Detection of spatial variability in relative density of fishes: comparison of visual census, angling, and baited underwater video. *Marine Ecology Progress Series*, *198*, 249–260.